Supporting information

A biomass based free radical scavenger binder endowing compatible cathode interface of 5 V lithium-ion battery

Yue Ma[†,‖+], Kai Chen[†+], Jun Ma[†], Gaojie Xu[†], Shanmu Dong[†], Bingbing Chen[†], Jiedong Li[†], Zheng Chen[†], Xinhong Zhou[‡], Guanglei Cui*[,†]

[†]Qingdao Industrial Energy Storage Research Institute, Qingdao Institute of Bioenergy and Bioprocess Technology, Chinese Academy of Sciences, Qingdao 266101,P. R. China

[‖]University of Chinese Academy of Sciences, Beijing 100049, P. R. China

[‡]College of Chemistry and Molecular Engineering, Qingdao University of Science & Technology, Qingdao 266042, P. R. China

Lignin (**Figure S1a**) is a three-dimensional natural polymer with predominantly phenolic architecture to transport water and mineral substance, adding strength and rigidity to cell walls of almost all plants in nature. The abundant C content (over 60%) in lignin make it a promising candidate in paper and pulp industry through the ages.[1] It is known that phenolic antioxidant is a group of compounds that could devitalize the alcoxyl free radicals by reacting with them, and terminating the free radicals chain reaction as possible as it can. [2-4] Because of steric hindrance, the H in -OH group of lignin is more liable to fall off. Thereby, it devitalizes the alcoxyl free radicals by reacting with them and terminating the free radical chain reaction just as following formula (1) shown.

(1)
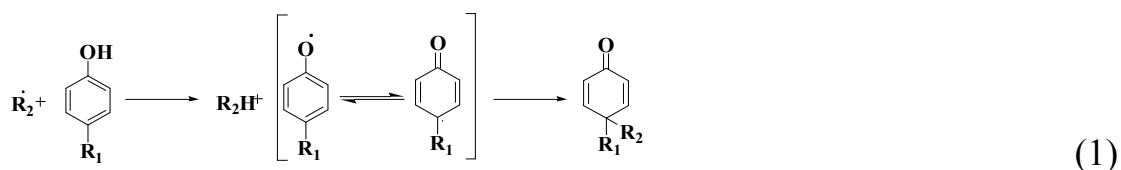
Better yet, numerous para-substituted groups exist in the phenol backbone and strengthen the free radical scavenge ability: the electron donating of substituted group can increase the charge density of oxygen on -OH, then accelerates the separation of hydrogen ions and oxygen atoms, increases the rate constant of reaction with the free radicals, reduces the electrophilic replacement constant of phenol free radicals, and augments the free radicals scavenge numbers ultimately.

The related Fourier transform infrared spectroscopy (FITR) spectrum of lignin is shown in **Figure S1a**. The broad peak at 3423 cm^{-1} is related to

O-H stretching vibration and the peaks at 1600 cm^{-1} corresponds to the C=C vibration in benzene ring. The peaks at 1424 cm^{-1} indicate the presence of C-H stretching, and the peaks at 1124 and 620 cm^{-1} are belonged to -SO$_3$H. The polymer with lower crystallinity can effectively transport the lithium ions, diminish the impedance and reduce the diffusion energy barrier, facilitating the reliable charge/discharge ability. Thermodynamic stability is also critical to the binder application in batteries. From TG files (**Figure S1b**) we can see that the lignin shows a good thermodynamic stability within the working range. The peeling strength is a requisite for electrode processing and the peeling comparison test of lignin and PVDF based electrode have been conducted and showed in **Figure S1c.** Compared to the PVDF electrodes (0.234 N mm^{-1}), lignin electrode delivers a little higher peeling strength (0.299 N mm^{-1}) owing to the abundant of -OH present in the backbone, which will provide more hydrogen bond. As a contrast, the binding ability of PVDF mainly originates from weak van der Waals interaction.[5] Besides, the processing of lignin electrode is environmentally benign by using water as solvent rather than using toxic organic solvent.
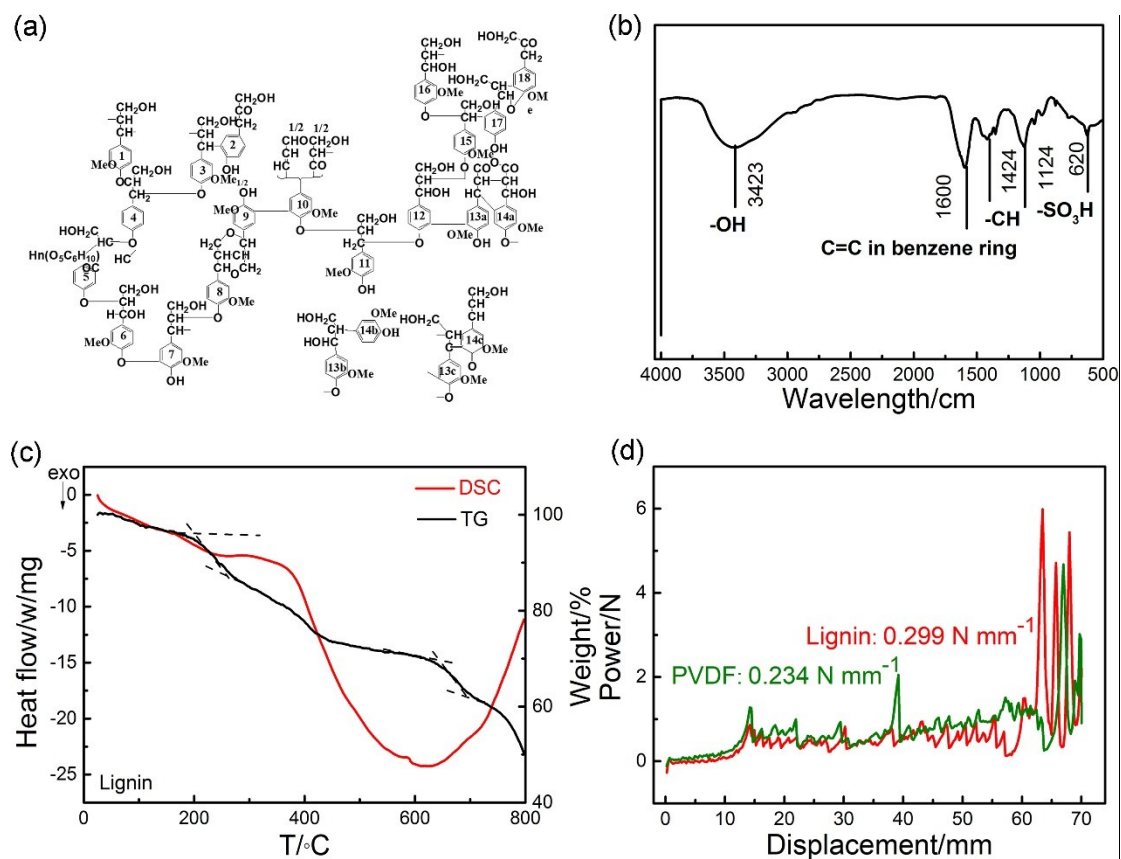
Figure S1. (a) Structure and (b) FTIR spectrum of lignin. (c) Thermogravimetric analysis result of lignin binder. (d) Average peeling forces measured from fresh lignin and PVDF based cathodes.
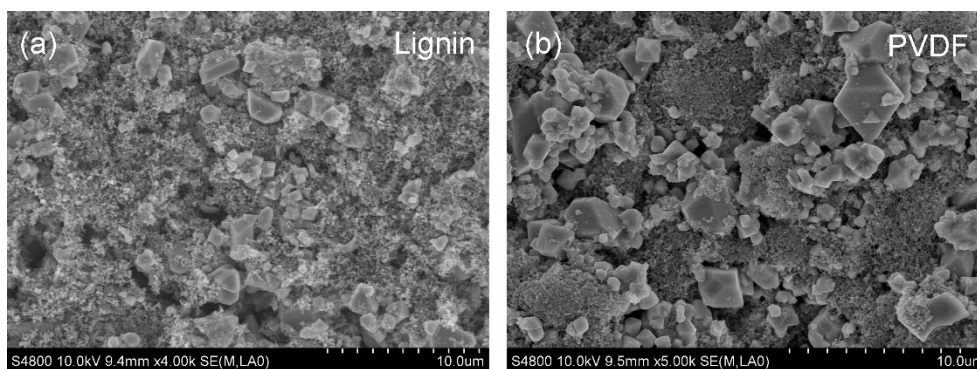
Figure S2. Typical SEM images of pristine (a) lignin and (b) PVDF based LNMO cathodes

To further elucidate the binding effect on the electrode surface, the pristine LNMO electrodes are surveyed by SEM imaging. As shown in **Figure S2a**, the surface of lignin based cathode exhibit smooth and dense surface morphology, while those with PVDF binder exhibit an uneven surface owing to the cluster of SP under the high viscosity effect of PVDF.
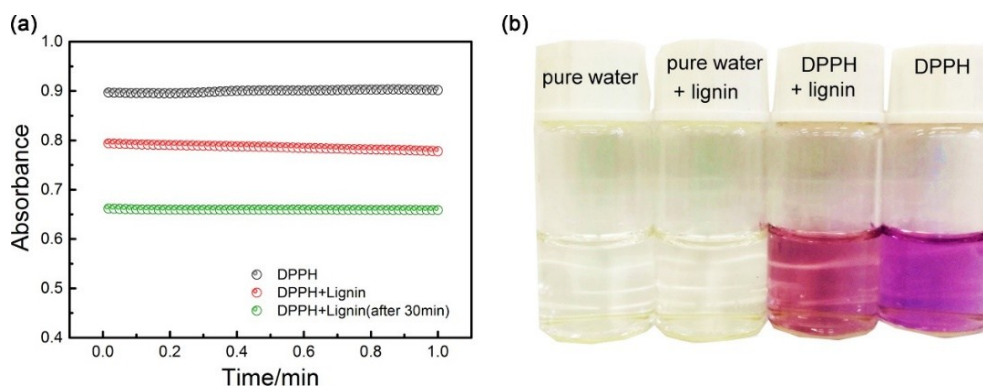
Figure S3. (a) UV-vis spectra of DPPH and DPPH+lignin. (b) Digital photographs of DPPH and DPPH+lignin

In **Figure S3**, Ultraviolet spectroscopy (UV) is conducted to further confirm the free radical scavenge role of lignin binder. In this section, 1,1-diphenyl-2-picrylhydrazyl (DPPH) is a stable free radical and often be used as an indicator of free radical scavenging. The UV absorbance of DPPH is depicted in **Figure S3a** in a black line. After adding the lignin, the value of absorbance profiles decreases, and reaches a constant value after 0.5 h, confirming the effective free radical trapping ability of lignin binder. Moreover, the much simpler and straightforward digital photographs of pure DPPH, lignin and DPPH/lignin mixture are vividly shown, which exhibit colorless, purple and deep pink color, respectively. This reflects the reaction between radicals and lignin visually. Deionized water is used as the counterpart. Alkyl free radicals will be generated after solvent molecules lose electron, and they are eliminated soon after contacting the lignin binder incorporated in the cathode region, then the relatively stable interfaces between cathode and electrolyte are formed.
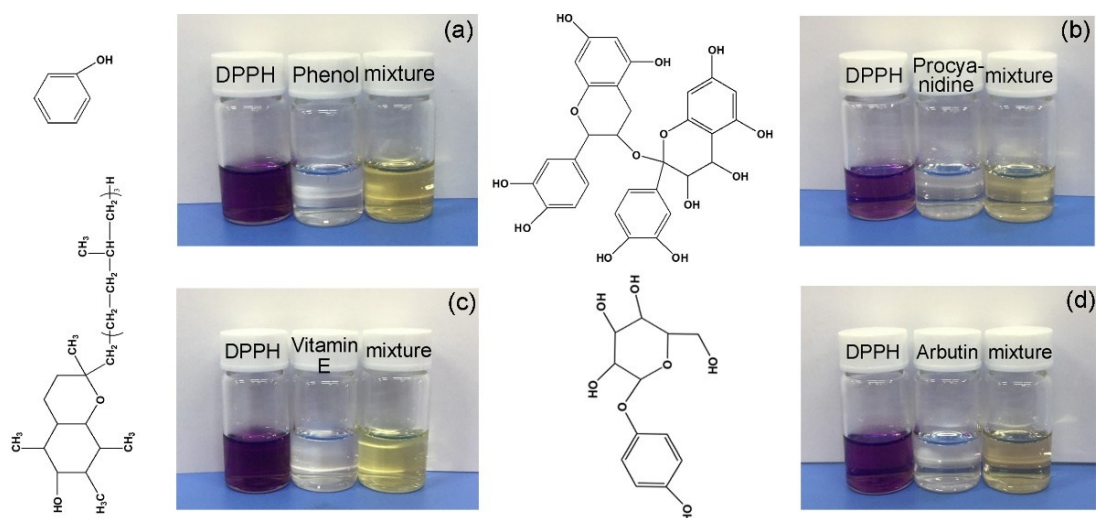
Figure S4. Digital photographs of DPPH and mixtures with (a) phenol, (b) procyanidine, (c) vitamin E, and (d) arbutin.

It is acknowledged that the phenol group could scavenge the free radicals. We select some natural materials (phenol, vitamin E, procyanidine, arbutin) with similar structure to the lignin. Their molecular weight is smaller than lignin (10,000). 1,1-diphenyl-2-picrylhydrazyl (DPPH) is used as indicator of the free radical scavenging ability of these candidates. The straightforward digital photographs of pure DPPH, phenol/DPPH, vitamin E/DPPH, procyanidine/DPPH and arbutin/DPPH mixture are compared in **Figure S4**. After adding the natural molecular into the DPPH solution, color evaluation can be observed in four samples, indicating the reduction of DPPH and the free radical scavenging capability of these renewable materials.
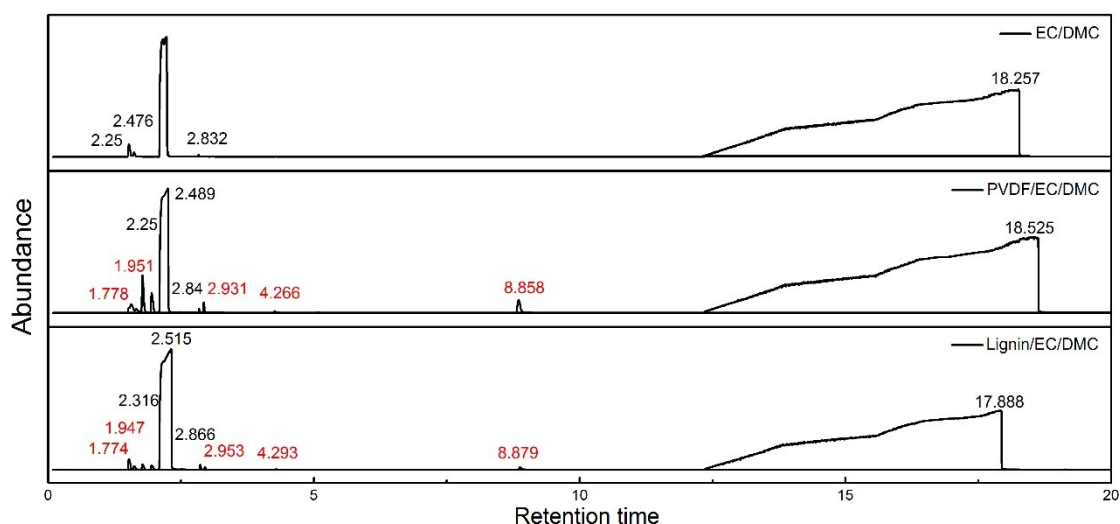
Figure S5. Gas Chromatography-Mass Spectrometer (GC-MS) of pure EC/DMC, PVDF/EC/DMC and lignin/EC/DMC

The fully-charged electrodes with lignin and PVDF binder are soaked in fresh EC/DMC solvent for 5 days and the obtained solvents are defined as lignin/EC/DMC and PVDF/EC/DMC, respectively. Then, GC-MS measurement is conducted on the fresh EC/DMC solvent and electrode soaked solvents. New species generated in lignin/EC/DMC and PVDF/EC/DMC, ascribing to the decomposition product of solvent. The peak area of newly formed peak in lignin/EC/DMC and PVDF/EC/DMC are normalized and compared. More by-products are formed in PVDF/EC/DMC and the specific data is listed in **Table S1**.
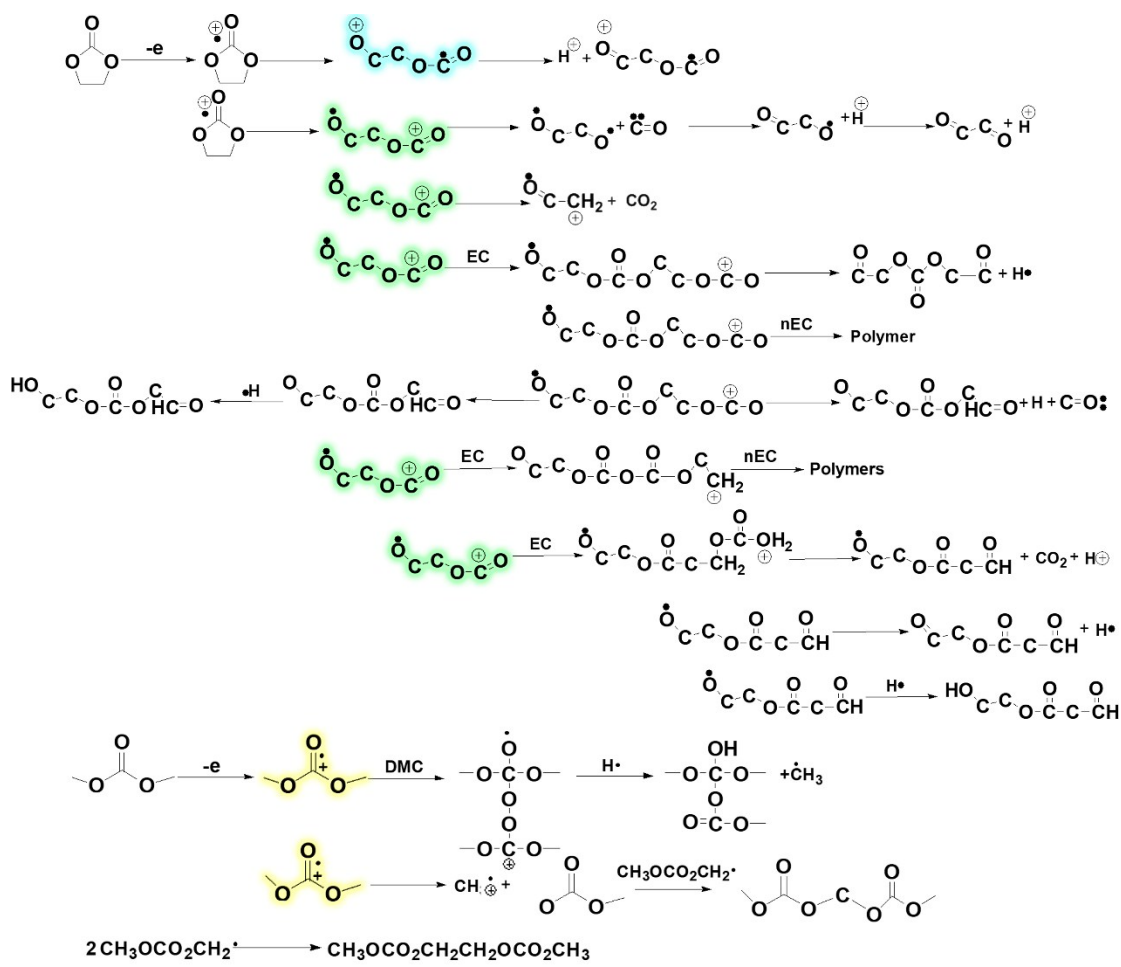
Figure S6. Possible EC and DMC oxidation patterns and follow-up reactions.[6]

The possible EC and DMC solvent oxidation patterns and follow-up reactions are demonstrated in **Figure S6** according to previous papers. The generation and the chain decomposition reaction of free radicals marked with highlight can be repressed by lignin binder, thus the solvent decomposition can be alleviated to a great extent.
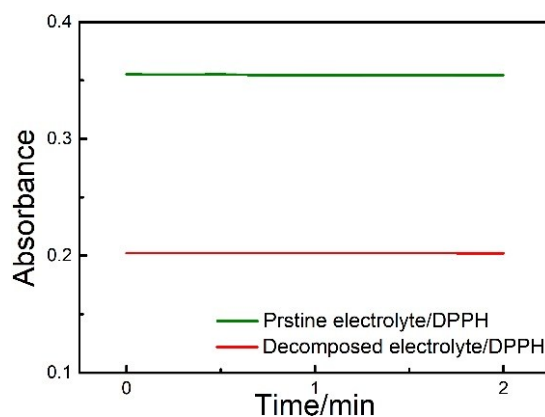
Figure S7. UV-vis spectra of pristine 1 M $LiPF_6$ in EC/DMC electrolyte solution/DPPH and decomposed 1M $LiPF_6$ in EC/DMC electrolyte solution/DPPH.

To characterize the generation of free radicals, three-electrode polypropylene cells were used for electrolysis: LNMO electrode was used as the working electrode and Li foil as reference electrode and counter electrode. The area of the working electrodes is 0.5 cm², and the distance between the electrodes is 0.4 cm. Electrolysis was carried out at 5 V using a potentiostat. 1 M $LiPF_6$ in EC/DMC electrolyte is used and the electrolyte solution is removed from the cell after electrolyzing for 1 min (referred as decomposed electrolyte solution) and 10 uL DPPH (5 wt.%) was added into the solution (DPPH is mentioned in supporting information and is a stable free radical and often be used as an indicator of free radical scavenging). The Ultraviolet spectrum (UV) absorbance of pristine electrolyte solution/DPPH and decomposed electrolyte solution/DPPH is depicted in **Figure S7**. The absorbance value of decomposed electrolyte solution/DPPH shows a remarkable lower value, indicating the reduction of effective DPPH indicator and the generation of free radicals, whose generation will reduce the concentration of DPPH by reacting with it.
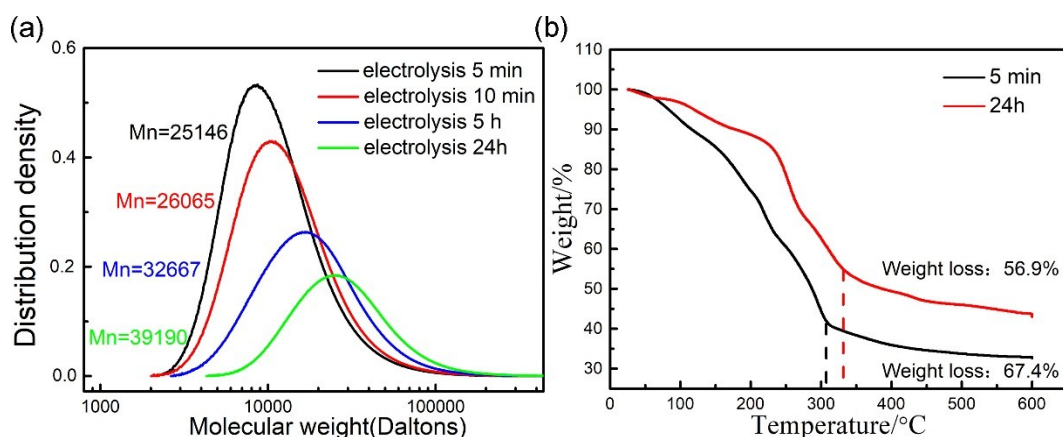
Figure S8. (a) Molecular weight distribution of the decomposed electrolyte residue after different electrolysis time obtained from GPC spectra. (b) Thermogravimetric (TG) profiles of electrolyte residue after 5 min and 24 h electrolysis time.

The chain propagation reaction producing the active alkyl radicals is considered to be a polymerization reaction which usually can be confirmed by GPC-LC technique.[7] Therefore, to characterize the radical propagation reaction, liquid chromatography (LC) measurements are used in our case. The electrolyte solutions were removed from the cell after charging for 5 min, 10 min, 5 h and 24 h, then were dried in vacuum and diluted with tetrahydrofuran (THF). After filtration by a 45 mm membrane filter, gel permeation chromatography liquid chromatography (GPC-LC) was performed using Breeze 2 HPLC system. It can be seen from **Figure S8** that the average molecular weight of decomposed electrolyte residue increases as the electrolysis time increases, indicating the propagation reaction of free radical.

Moreover, the electrolyte solution after 5 min and 24 h electrolysis time are dried in vacuum and the thermogravimetric (TG) profiles of residue are

investigated in **Figure S8b**. Electrolyte solution after 24 h electrolysis time exhibits a weight loss of 56.9% at the inflection temperature of 340 ℃, lower than that of 67.4% (inflection temperature of 311 ℃) for electrolyte solution after 5 min electrolysis time, indicating that the molecular weight of electrolyte residue after 24 h electrolysis time is higher than that of 5 min counterpart. These results coincide with the result of GPC, suggesting the chain propagation reaction of free radical.
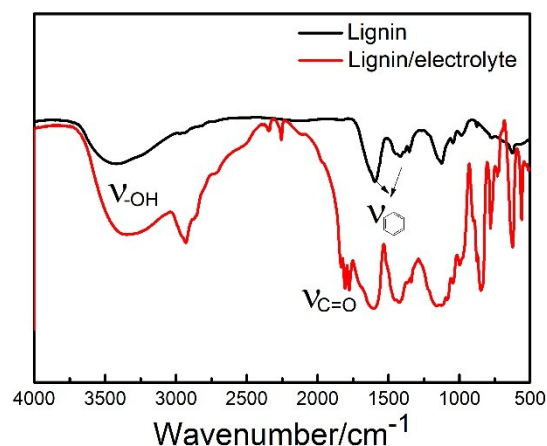
Figure S9. FTIR spectra of pristine lignin powder and recycled lignin powder from the electrolyte of 1 M $LiPF_6$ in EC/DMC after electrolysis.

To test the radical transfer to the lignin, we added lignin powder into electrolyte (referred as lignin/electrolyte) and electrolysis was carried out at 5 V using a potentiostat within 1 h. Then the lignin powder was removed from the cell and dried in vacuum. In FTIR spectra of **Figure S9**, new peak corresponding to the vibration of C=O can be observed, indicating the transfer of carbonic ester caused by free radical to the lignin molecular.
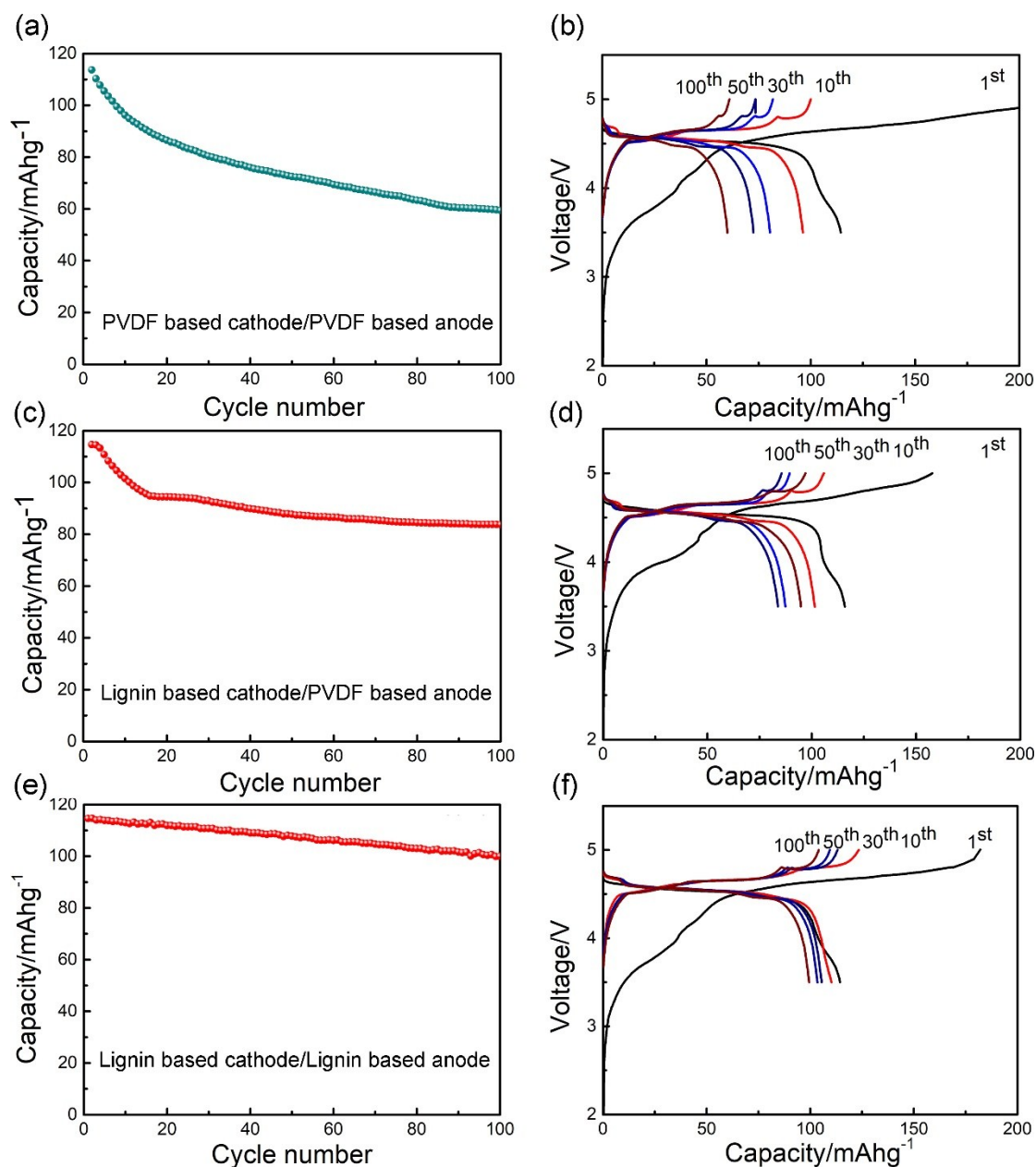
Figure S10. Effects of lignin and PVDF binder on cycling performance of LNMO/graphite full-cells: (a) PVDF based cathode/PVDF based anode, (c) lignin based cathode/PVDF based anode, (e) lignin based cathode/lignin based anode. Charge-discharge profiles of full-cells with (b) PVDF based cathode/PVDF based anode, (d) lignin based cathode/PVDF based anode and (f) lignin based cathode/lignin based anode at 1 C (1 C = 150 mA g^{-1}).

The electrochemical performance of the lignin and PVDF based electrodes is evaluated in LNMO/graphite full-cells. As shown in **Figure**

S10a and **10b**, the full-cell with PVDF based cathode and anode only delivered a discharge capacity of 60 mAh g^{-1} after 100 cycles, while the full-cell with lignin based cathode/PVDF based anode delivered a higher capacity of 80 mAh g^{-1} in **Figure S10c** and **10d**. The full-cell with lignin based cathode exhibits a lower charge/discharge voltage polarization and a higher capacity retention with the elapsed time. When the lignin binder is used in anode in **Figure S10e** and **10f**, the capacity maintained 98.9 mAh g^{-1} after 100 cycles, the significant performance improvement may ascribe to the free radical scavenge capability of lignin throughout the whole battery system.

The cycling profiles of LNMO/graphite full-cell is totally different from that of LNMO/Li cell because any parasitic reaction might occur in the full-cell, which cause the irreversible capacity fading.[8] The capacity decay mechanism in LNMO/graphite full-cell might be explained by the following reasons: a) electrolyte oxidation at the interface of LNMO, b) migration of the side-reaction products toward the graphite anode, and c) consumption of Li$^+$ at the electrolyte/graphite interface. Moreover, several other issues, including co-intercalation of side-reaction products into graphite, which leads to its exfoliation, and shuttling of CO_2, have been suggested to occur. [9] The instability of carbonate-based conventional electrolytes at high voltages would be a critical issue. However, it is not the only source of concern for the implementation of LNMO/graphite full-

cells. Several other issues including the corrosion of conductive carbon, separator and stainless steel, the matching technology of anode and cathode electrode could potentially degrade LNMO/graphite full-cell performance. [10-11] The purpose of our work is to reduce the electrolyte decomposition on cathode side from the viewpoint of binder. To improve the performance of full-cell, approaches including electrode coating, electrolyte additives, blocking/scavenging membranes and new electrolyte solvents might be adopted in the future work.
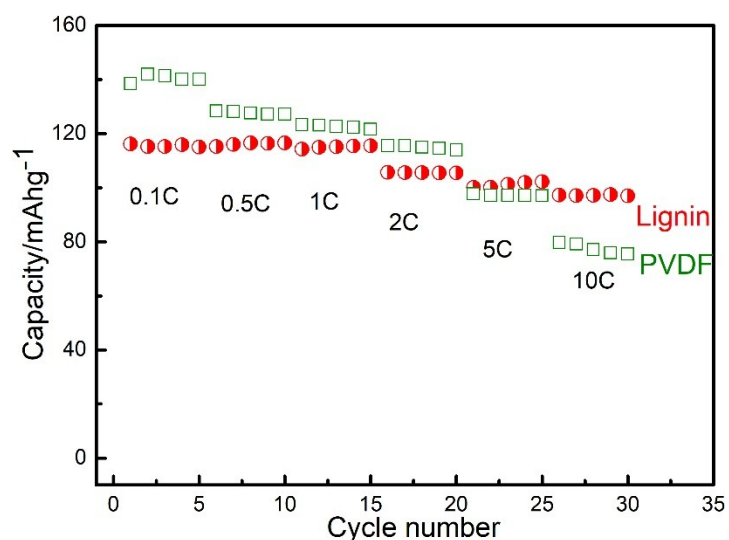
Figure S11. The discharge capacity of LNMO half-cell with lignin and PVDF binder at varied rates.

The lignin based battery demonstrates superior rate capability at higher current densities (0.1 C: 116.1 mAh g^{-1}, 0.5 C: 115.2 mAh g^{-1}, 1 C: 114.2 mAh g^{-1}, 2 C: 105.6 mAh g^{-1}, 5 C: 100.1 mAh g^{-1}, 10 C: 97.2 mAh g^{-1}, respectively in **Figure S11** than that of PVDF based battery (130.9 mAh g^{-1}, 125.1 mAh g^{-1}, 123.2 mAh g^{-1}, 109.5 mAh g^{-1}, 97.6 mAh g^{-1}, 79.7 mAh g^{-1}, respectively).
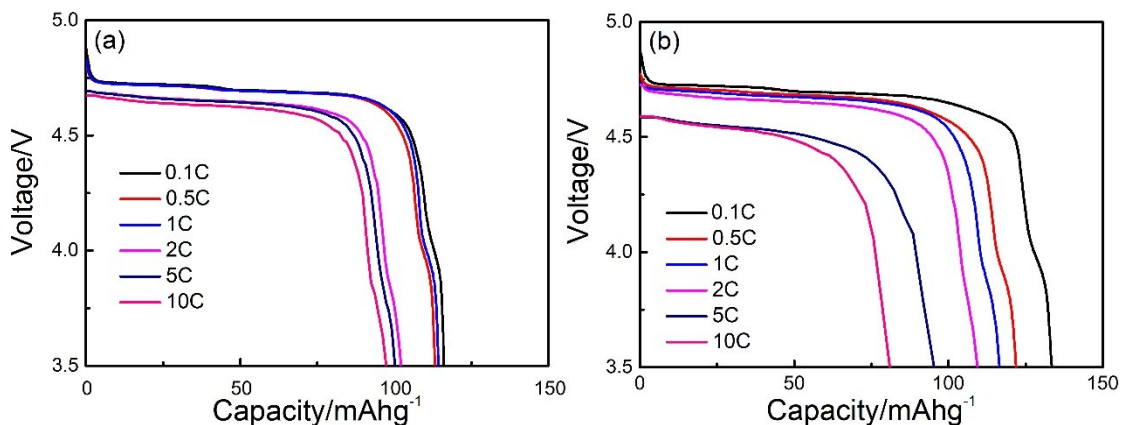
Figure S12. The corresponding charge/discharge profiles of the (a) lignin and (b) PVDF based electrodes at varied current rates (3.5-5.0 V vs. Li$^+$/Li).

In **Figure S12**, the discharge profiles of lignin and PVDF based batteries at different rates are presented for comparison. The polarization of discharge curves increases with the increasing rate while the capacity decreases. In lignin based electrode, a capacity value of 116.1 mAh g^{-1} is delivered at 0.1C and kept at 97.2 mAh g^{-1} at 10 C. In a sharp contrast, only 130.9 mAh g^{-1} is delivered for PVDF based battery at 0.1C rate and only 79.7 mAh g^{-1} at 10 C. At all current densities, the lignin based electrode exhibits lower charge/discharge voltage polarization, indicating better conductivity and lower overall resistance.
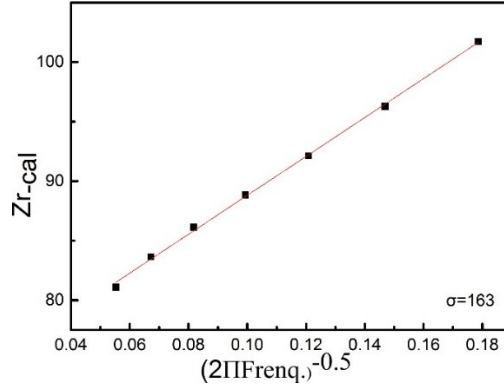
Figure S13. The diffusion coefficient of lignin based electrode.

The diffusion coefficient of lignin based electrode is exhibited in the following Figure S13. In order to verify the diffusion of lithium ions through the electrode, the diffusion coefficient is calculated by Electrochemical impedance spectroscopy (EIS). A volume value of Zr-cal can be observed. Take Zr-cal as Y axis, $(2\pi*Frency)^{-1/2}$ as X axis, then a constant can be obtained by fitting the line. According to the following formula: $D_{Li+}=R^2T^2/2A^2n^4F^4C^2\sigma^2$, where R is the gas constant, T is the absolute temperature, A is the surface area of the cathode (1 cm^2), n is the number of electrons transferred in the half-reaction for the redox couple, which is equal to 1, F is the Faraday constant, C is the concentration of Li ion in solid (4.37×10^{-3} mol cm^{-3}), D is the diffusion coefficient (cm^2 s^{-1}), and σ is the Warburg factor, which is relative to Z re. σ can be obtained from the slope of the lines. Finally, the diffusion coefficient value of 9.45 $\times 10^{-12}$ cm^2 s^{-1} can be worked out, which is 1.5 times that of 6.0×10^{-12} cm^2 s^{-1} for PVDF counterpart.
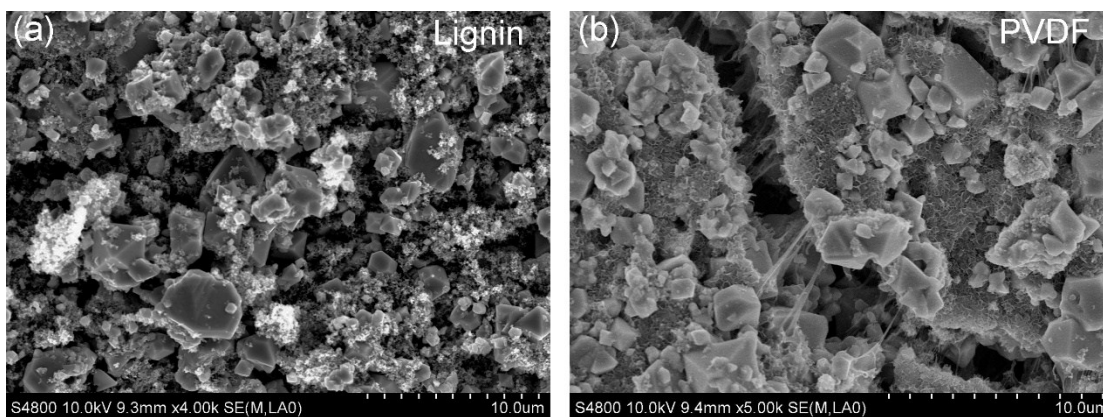
Figure S14. Typical SEM images of lignin (a) and PVDF (b) based cathodes after cycling.

After long cycling, the surfaces of the cathodes after cycling exhibit different morphologies. The lignin based electrode is still intact and uniform, while the PVDF based electrode suffers a severe structural damage. This is consistent with previous cycling data, that is to say, the lignin binder could provide superior binding capability and improve the Coulombic efficiency as well as long cycling stability.
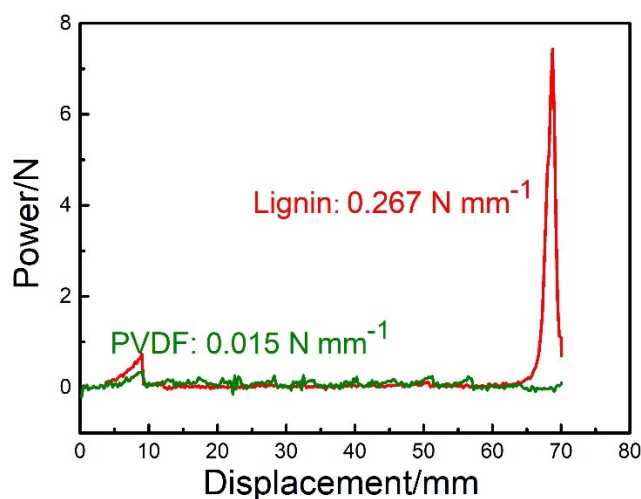
Figure S15. Average peeling forces measured from cycled lignin and PVDF based electrodes.

After cycling, a peeling strength of 0.267 N mm^{-1} is maintained for lignin based electrode, while the peeling strength of PVDF counterpart is 0.015 N mm^{-1}. These results demonstrate the stronger binding capability of lignin binder.
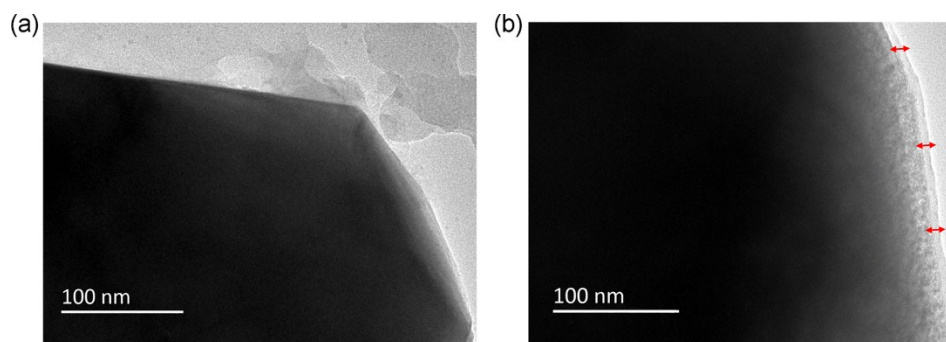
Figure S16. HR-TEM images of (a) pristine electrode and (b) electrode after cycling.

The pristine LNMO particle demonstrate a smooth edge just like **Figure S16a** shown, while after cycling, the electrolyte decomposition is suppressed by lignin and less decomposition species generated on the particles and result in the relatively thin and uniform coverage on the surface of LNMO particle (**Figure S16b**), which is usually referred as CEI. The thick of CEI is usually about 5-10 nm.
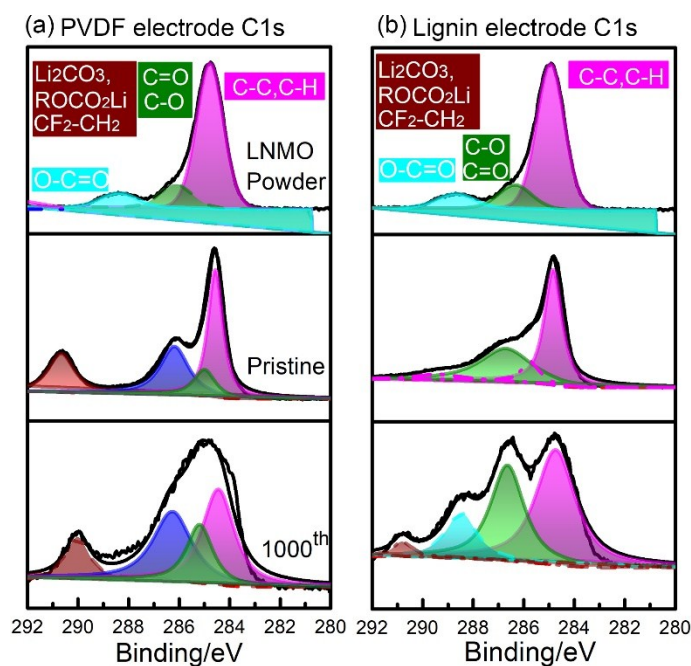
Figure S17. High resolution C1s XPS spectra of LNMO electrodes based on (a) PVDF and (b) lignin binder before and after 1000 cycles.

The pure LNMO powder shows characteristic peak of inherent hydrocarbon. As for cycled PVDF based electrode, the peaks centered at 290.5 eV belong to the generation of electrolyte decomposition byproduct $ROCO_2Li$ and Li_2CO_3 species, while the newly formed peaks centered at 286.9 eV correspond to alkyl group with carbonate oxygen (O=C-O) and carbonyl compound (C=O) yield from decomposition of electrolyte solvent. [12] The lignin based electrode contains peaks of O=C-O, C=O (286.0 eV - 287.0), and C-O (288.8 eV). Specifically, the relative intensity of C-O peak in the lignin based electrode is higher, ascribing to the initial presence of C-O group in lignin backbone. Besides, the peak intensity at 290.0 eV is lower in lignin based electrode, indicating less $ROCO_2Li$ and Li_2CO_3 species generated and less side reaction occured.
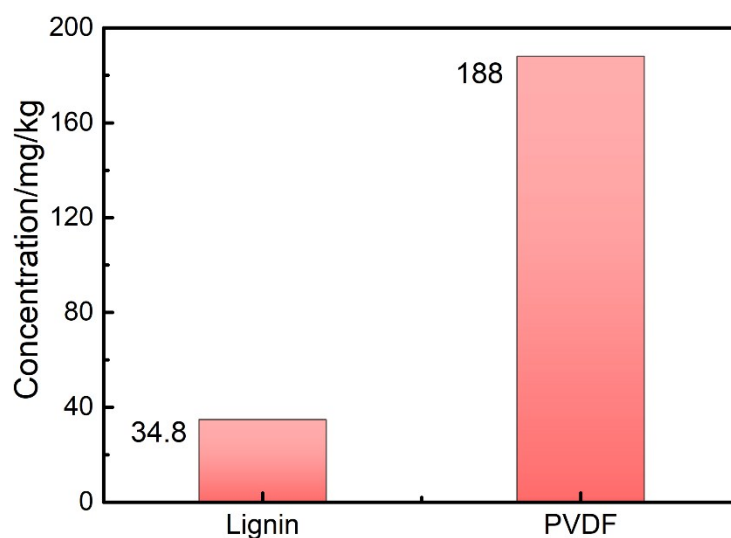
Figure S18. ICP-MS results of Mn^{2+} ions in the electrolytes from lignin and PVDF based electrodes.

The LNMO electrodes are assembled in half-cell and charged to 5.0 V, then unpacked the battery and soaked the LNMO electrode in liquid electrolyte to investigate the dissolution of transition metal. In electrolyte solvent with lignin based electrode, the Mn ion content is 34.8 ppm, which is far lower than that of PVDF (188 ppm), demonstrating the alleviated Mn ion dissolution in the lignin based electrode.
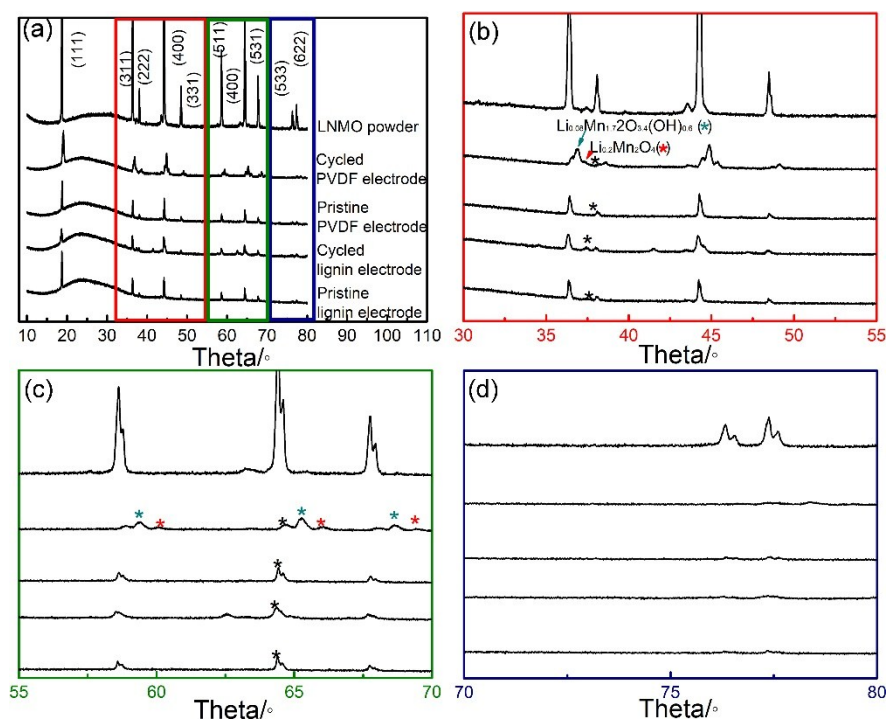
Figure S19. X-Ray diffraction patterns of LNMO powder, pristine and cycled PVDF based electrode, pristine and cycled lignin based electrode. Magnified views of selected regions are shown in (b), (c) and (d). The black star stands for Al signal.

Figure S19 shows the X-ray diffraction (XRD) patterns of disordered $Fd\bar{3}m$ LiNi$_{0.5}$Mn$_{1.5}$O$_4$ at pristine state and fully-charged state after long-term cycling with lignin and PVDF binder. XRD characteristic peaks can be compared to elaborate the transition metal dissolution and the electrode structure evaluation.[13] In **Figure S19a**, characteristic peaks of disordered $Fd\bar{3}m$ LNMO is marked, three highest intensity peaks at 18.6 °, 36.5 ° and 44.4 ° belong to (111), (311) and (400). The peaks positioned at 38.4 °, 49.1 °, 59.2 °, 65.4 ° and 68.8 °correspond to (222), (331), (400), (511) and (531), respectively. The two electrodes in pristine state present similar XRD characteristic with pure LNMO powder. Then the entire test area is magnified in **Figure S19b**, **S19c** and **S19d** to better observe the lattice

evolution for lignin and PVDF based electrodes before and after 1000 cycles. Noting that the black star in the enlarged figures stands for the signal of aluminum foil. In characteristic peaks of cycled PVDF based electrode shown in **Figure S19b**, two new peaks appeared at 36.7 ° and 37.1 °, which belong to the $Li_{0.08}Mn_{1.72}O_{3.4}(OH)_{0.6}$ and $Li_{0.2}Mn_2O_4$ phase according to PDF card 89-0754 and 84-1524. The additional peaks at 45.1 ° and 45.3 ° are also related to $Li_{0.08}Mn_{1.72}O_{3.4}(OH)_{0.6}$ and $Li_{0.2}Mn_2O_4$ phase, respectively. Thus the new phase of $Li_{0.08}Mn_{1.72}O_{3.4}(OH)_{0.6}$ and $Li_{0.2}Mn_2O_4$ are marked by green and red stars in the following discussion. Similarly, the new peaks assigned to $Li_{0.08}Mn_{1.72}O_{3.4}(OH)_{0.6}$ can be observed at 59 °, 65.5 °and 68.1° in **Figure S19c**, while the peaks at 60 °, 66.2 ° and 68.9 ° are attributed to $Li_{0.2}Mn_2O_4$. In **Figure S19d**, for cycled PVDF based electrode, the crystal face of (533) and (622) vanishes while the cycled lignin based electrode maintains the initial state after cycling. Therefore, we can deduce that with the decomposition of electrolyte, the lattice structure of PVDF based electrode degraded and the new Mn-contained phase formed by the mutual effect of Mn dissolution, solvent decomposition and irreversibly lithiation. On account of the free radical scavenging capacity, lignin effectively suppresses the decomposition of electrolyte, thereby prevents the active material from by-product attacking, and establishes stable interface between electrode and electrolyte.
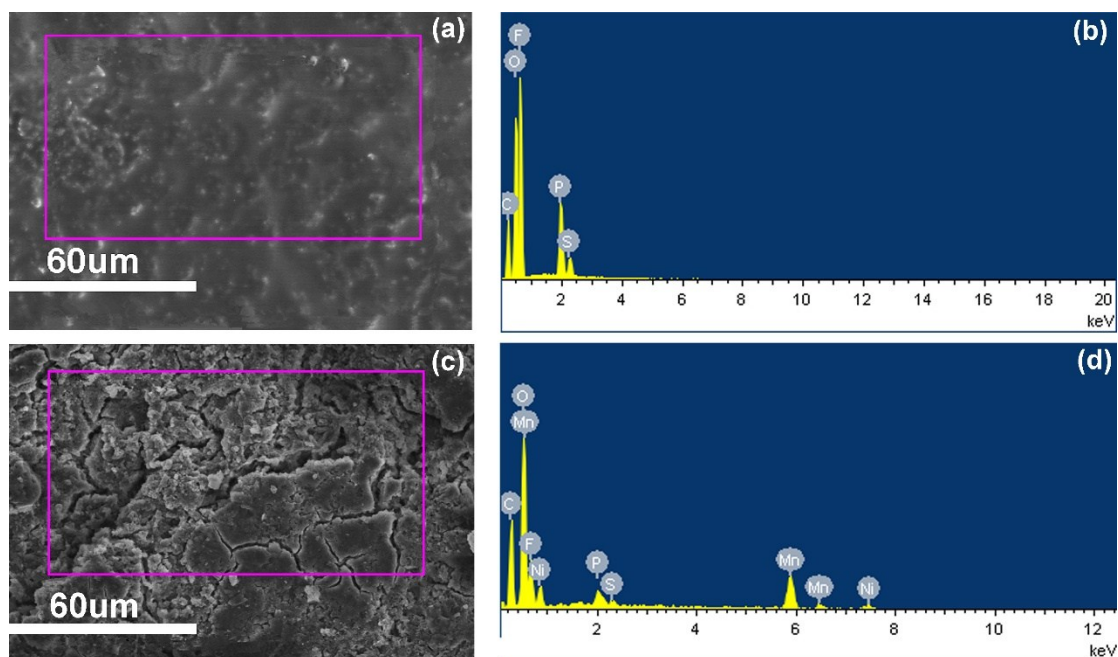
Figure S20. Typical SEM image of lithium foils obtained from (a) lignin half-cell and (b) the related Energy Dispersive Spectrum (EDS) spectra. SEM image of lithium foils obtained from (c) PVDF half-cell and (d) the related EDS spectra.

Figure S20a and **20c** show the typical SEM images of the lithium foils from lignin and PVDF half-cells. **Figure S20a** shows compact and homogeneous morphology while **Figure S20c** reveals an unevenness lithium foil surface with massive cracks. According to the EDS spectra shown in **Figure S20b** and **20d**, Mn and Ni elements appear on the surface of lithium foil from PVDF half-cell, suggesting a severe dissolution of transition elements.
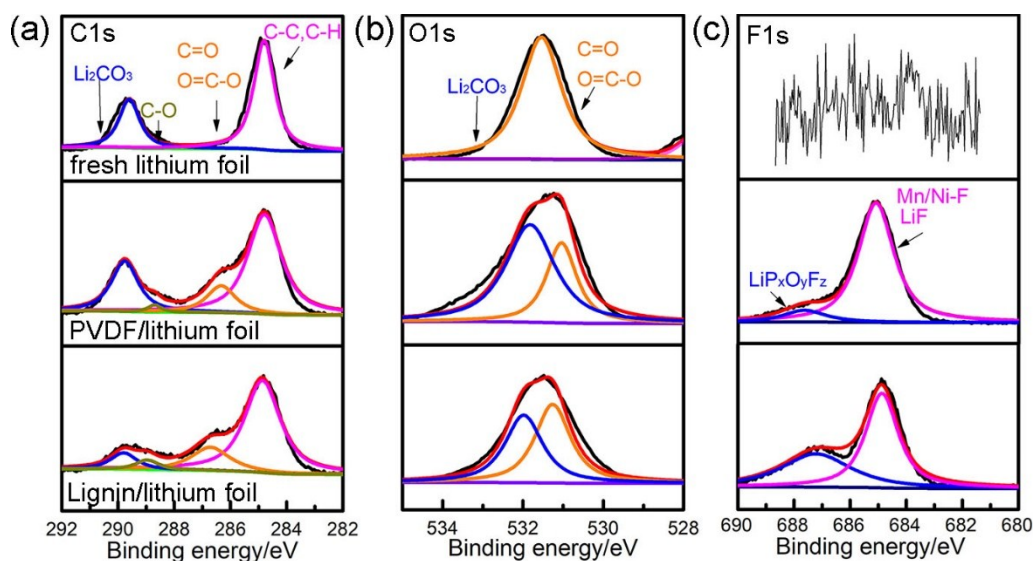
Figure S21. The surface composition of lithium foils from lignin and PVDF half-cells probed by high-resolution XPS measurements: C1s (a), O1s (b) and F1s (c) after cycling.

The C1s spectra of lithium foils from lignin and PVDF half-cell after 500 cycles are shown in **Figure S21**. The O1s spectra and F1s spectra are also compared to evaluate the side reaction occurred on the surface of lithium foils. In C1s spectra and O1s spectra, more Li_2CO_3 and $ROCO_2Li$ generated in the PVDF half-cell, indicating more severe solvent decomposition. In F1s spectra, higher amount of species containing Mn or Ni element generated on the surface of lithium foils PVDF half-cell.

Table S1. GC-MS data of EC/DMC, EC/DMC/PVDF, EC/DMC/Lignin

EC/DMC		EC/DMC/PVDF			EC/DMC/Lignin		
Retention Time	Area	Retention Time	Area	ratio	Retention Time	Area	ratio
2.225	1.63E+09	1.778	1.490E+08	**5.560E-03**	1.774	28482008	**1.330E-03**
2.476	2458698	1.951	80750355	**3.010E-03**	1.947	24525057	**1.150E-03**
2.832	4843932	2.255	1.980E+09		2.316	2.85 E+10	
18.257	2.37E+10	2.489	3324697		2.515	3485966	
		2.84	8967144		2.866	12015227	
		2.931	23914384	**8.910E-04**	2.953	7248548	**3.400E-03**
		4.266	5898191	**2.200E-04**	4.293	2221689	**1.040E-04**
		8.858	87854298	**3.270E-03**	8.879	18346525	**8.600E-04**
		18.525	2.680E+10		17.888	2.13 E+10	

In order to lucubrate the interface reaction between fully-charged cathode and electrolyte, gas chromatography-mass spectrometer (GC-MS) is employed to detect the decomposition byproduct of electrolyte solvent and the results are displayed in **Table S1**. In pristine EC/DMC solution, four peaks are exhibited. After adding fully-charged lignin and PVDF based electrodes, five new peaks are formed and the intensity value of newly formed peaks are normalized and write in red bold. EC/DMC/PVDF shows a higher intensity value, indicating much electrolyte solvent are badly decomposed.

Table S2. Peak assignment of F1s spectra.

Binding energy (eV)	Peak assignment
685.5	LiF, MnF_2, NiF_2
686.5	$LiPO_yF_z$, Li_xPF_y
687.9-688.1	$(-CF_2CH_2-)n$

Table S3. Peak assignment of C1s spectra.

Binding energy (eV)	Peak assignment
284.5	$(-CH_2CH(C(O)OCH_2CF_3)-)n$, C-C
285.7	$(-CF_2CH_2-)n$, C-O
286.8	$-CH(OH)$,$(-CH_2C(O)O-)n$, $(-CH_2-CF_2-)n$ $(((-CH_2CH_2-)x)-CH_2CH_2OC(O)O-)n$
287.5	C=O, O-C-O
288.8	O-C=O,
290	Li_2CO_3; $ROCO_2 Li$; $CH_2-C* F_2$ from PVDF

Table S4. Peak assignment of O1s spectra.

Binding energy (eV)	Peak assignment
529.7	Lattice oxygen of $LiNi_{0.5}Mn_{1.5}O_4$
531-532	C=O; O-C=O, O-C-O; Li_2CO_3 ;$ROCO_2 Li$,
532.9	C-O

References

1. Nirmale, T. C.; Kale, B. B.; Varma, A. J., A review on cellulose and lignin based binders and electrodes: Small steps towards a sustainable lithium ion battery. *Int. J. Biol. Macromol.* **2017,** *103*, 1032-1043.

2. Vulic, I.; Vitarelli, G.; Zenner, J. M., Structure-property relationships: phenolic antioxidants with high efficiency and low colour contribution. *Polym. Degrad. Stab.* **2002,** *78* (1), 27-34.

3. Ohkatsu, Y.; Matsuura, T.; Yamato, M., A phenolic antioxidant trapping both alkyl and peroxy radicals. *Polym. Degrad. Stab.* **2003,** *81* (1), 151-156.

4. Villano, D.; Fernandez-Pachon, M. S.; Moya, M. L.; Troncoso, A. M.; Garcia-Parrilla, M. C., Radical scavenging ability of polyphenolic compounds towards DPPH free radical. *Talanta* **2007,** *71* (1), 230-5.

5. Lee, Y. H.; Min, J.; Lee, K.; Kim, S.; Park, S. H.; Choi, J. W., Low molecular weight spandex as a promising polymeric binder for $LiFePO_4$ Electrodes. *Adv. Energy Mater.* **2017,** *7* (8).

6. Moshkovich, M., Cagocaru. M., Gottlieb,H.E., Aurbach, D. The study of the anodic stability of alkyl carbonate solutions by in situ FTIR spectroscopy, EQCM, NMR and MS. *J. Electroanal.*

Chem. **2001,** *497*, 84-96.

7. Endo, E.; Ata, M.; Sekai, K.; Tanaka K. Spin trapping study of gradual decomposition of electrolyte solutions for Lithium secondary batteries. *J. Electrochem. Soc*. **1999**, *146 (1)*, 49-53.

8. Kim, J.-H.; Pieczonka, N. P. W.; Yang, L. Challenges and approaches for high-voltage spinel Lithium-ion batteries. *ChemPhysChem* **2014**, *15*, 1940-1954.

9. Chusid, O. Y.; Ely, E. E. ; Aurbach, D.; Babai, M.; Carmeli, Y. Electrochemical and spectroscopic studies of carbon electrodes in lithium battery electrolyte systems. *J. Power Souces* **1993**, *43(1-3)*, 47-64.

10. Patoux, S.; Daniel, L.; Bourbon, C.; Lignier, H.; Pagano, C.; Cras, F. L.; Jouanneau, S.; Martinet, S. High voltage spinel oxides for Li-ion batteries: From the material research to the application. *J. Power Souces* **2009***,189*, 344-352.

11. Pieczonka, N. P. W.; Liu, Z.Y.; Lu, P.; Olson, K. L.; Moote, J.; Powell, B. R.; Kim, J.-H. Understanding transition-metal dissolution behavior in $LiNi_{0.5}Mn_{1.5}O_4$ high-voltage spinel for Lithium ion batteries. *J. Phys. Chem. C* **2013**, *117*, 15947-15957.

12. Andersson, A.; Abraham, D.; Haasch, R.; MacLaren, S.; Liu, J.; Amine, K. Surface characterization of electrodes from high power lithium-ion batteries. *J. Electrochem. Soc.* **2002**, *149* (10), A1358-A1369.

13. Liu, D.; Zhu, W.; Trottier, J.; Gagnon, C.; Barray, F.; Guerfi, A.; Mauger, A.; Groult, H.; Julien, C. M.; Goodenough, J. B.; Zaghib, K., Spinel materials for high-voltage cathodes in Li-ion batteries. *RSC Adv.* **2014,** *4* (1), 154-167.